AIP | Journal of Applied Physics

Comparison of periodic light-trapping structures in thin crystalline silicon solar cells

Jo Gjessing, Aasmund S. Sudbø, and Erik S. Marstein

Citation: J. Appl. Phys. **110**, 033104 (2011); doi: 10.1063/1.3611425
View online: http://dx.doi.org/10.1063/1.3611425
View Table of Contents: http://jap.aip.org/resource/1/JAPIAU/v110/i3
Published by the American Institute of Physics.

Comparison of periodic light-trapping structures in thin crystalline silicon solar cells

Jo Gjessing,[1,2,3,a)] Aasmund S. Sudbø,[3] and Erik S. Marstein[3]
[1]*Institute for Energy Technology, Department of Solar Energy, P.O. Box 40, Kjeller 2027, Norway*
[2]*University of Oslo, Department of Physics, P.O. Box 104 8 Blindern, Oslo 0316, Norway*
[3]*University Graduate Center at Kjeller, P. O. Box 70, Kjeller 2027, Norway*

(Received 6 April 2011; accepted 17 June 2011; published online 4 August 2011)

Material costs may be reduced and electrical properties improved by utilizing thinner solar cells. Light trapping makes it possible to reduce wafer thickness without compromising optical absorption in a silicon solar cell. In this work we present a comprehensive comparison of the light-trapping properties of various bi-periodic structures with a square lattice. The geometries that we have investigated are cylinders, cones, inverted pyramids, dimples (half-spheres), and three more advanced structures, which we have called the roof mosaic, rose, and zigzag structure. Through simulations performed with a 20 μm thick Si cell, we have optimized the geometry of each structure for light trapping, investigated the performance at oblique angles of incidence, and computed efficiencies for the different diffraction orders for the optimized structures. We find that the lattice periods that give optimal light trapping are comparable for all structures, but that the light-trapping ability varies considerably between the structures. A far-field analysis reveals that the superior light-trapping structures exhibit a lower symmetry in their diffraction patterns. The best result is obtained for the zigzag structure with a simulated photo-generated current J_{ph} of 37.3 mA/cm^2, a light-trapping efficiency comparable to that of Lambertian light-trapping. © *2011 American Institute of Physics*. [doi:10.1063/1.3611425]

I. INTRODUCTION

Light trapping increases current generation in solar cells and makes it possible to reduce material costs by utilizing thinner solar cells. In addition to the reduced material consumption, a thinner solar cell also relaxes the demand on material quality as the dependence of efficiency upon bulk recombination is reduced. Light trapping is, therefore, a key issue of reaching the ambitious cost reduction plans for the photovoltaic (PV) industry.

Nowadays, state-of-the-art silicon (Si) solar cells have a thickness of around 150-200 μm. Fabrication of significantly thinner sheets of high quality Si with a thickness below 20 μm has been demonstrated by various techniques.[1–3] Throughout this work, we use a Si thickness of 20 μm as a case of study when exploring the light-trapping ability of the various structures. This is thinner than today's wafer-based solar cells by a factor of 10 and at the same time thicker than ordinary thin-film solar cells by a factor of 10. With proper light trapping, a Si solar cell with such a thickness has the potential of reaching high conversion efficiencies. This is crucial, due to the high importance of efficiency in determining the cost of a PV system. Working with an optical solar cell model, we use the photo-generated current density instead of conversion efficiency as a measure of light-trapping quality, as this requires fewer assumptions about the specific cell configuration.

Conventional light trapping varies according to cell type and configuration. For monocrystalline Si, alkaline etching of a [100] oriented wafer is used to make a texture of square pyramids with the {111} planes revealed.[4] Alkaline etching may also be used for multicrystalline Si, but due to the random orientation of the crystal grains, isotropic acidic etching that results in a random dimple-like pattern is a more common approach.[5] Pyramidal structures have been demonstrated on crystalline Si solar cells with thickness in the 30 micron range[6] despite structure sizes with a depth of more than 10 μm. These structures have excellent anti-reflection properties, but better light confinement may be achieved with other structures. Moreover, pyramidal structures are not applicable to proton cleaved wafers, which is a method for making very thin kerf-free wafers.[3] These wafers have a [111] oriented surface, while the conventional pyramidal texture requires a [100] oriented surface.

In thin-film solar cells, texturing of transparent conductive oxides (TCOs) on glass substrates is the common approach for light trapping.[7] This creates a random submicron texture, which effectively scatters light, especially at shorter wavelengths.

II. BACKGROUND

Periodic structures with lattice periods in the range of the wavelength of light are compatible with thin solar cells, and they unlock a potential outside the conventional light-trapping based on random textures. Such structures have been thoroughly analyzed in the past,[8–10] but have attracted renewed attention lately.[11–14] Recently, it has been shown that periodic structures may increase light trapping beyond that of the Lambertian $4n^2$ limit,[15,16] but with a significant angular dependency. At the same time, it has also been shown that bi-periodic gratings, in general, are expected to

[a)]Author to whom correspondence should be addressed. Electronic mail: jo.gjessing@ife.no.

have a higher potential than uni-periodic gratings. Lately, we have seen simulation results that are comparable to the geometric light-trapping limit over a broad wavelength range for bi-periodic gratings.[16–19] Common for these structures is that the Lambertian light-trapping limit is exceeded at normal incidence, while the Lambertian limit, although theoretical, is independent of incidence angle.

Light trapping from periodic structures have also been verified in experimental work. It has been shown that there is good agreement between modeling and experimental results for a uni-periodic grating applied to a 5 μm thick Si cell.[20] Recently, light trapping obtained from a periodic plasmon structure has been shown to exceed that of the Asahi U-type glass,[21] which is the thin-film solar cell standard. A similar result is also presented in Ref. 22. They found that a self-assembled periodic dimple structure made by anodic oxidation of Al improved light trapping in the infrared part of the spectrum above that of the Asahi U-type glass.

In this work, we investigate, in simulations, the impact of the specific unit cell geometry on seven different bi-periodic diffractive structures with regard to light trapping. The structures comprise the binary cylinder structure;[14] common non-binary structures, such as inverted pyramids, cones, and dimples, or half spheres; and, finally, three more advanced structures, which we call the roof-mosaic structure, the rose structure,[23] and the zigzag structure.[24] Some of these structures have also been investigated before. Modeling of coexisting front- and back-side pyramids is presented in Ref. 25; modeling results of cylinders are presented in several works,[12,14,26,27] while modeling of cones is performed in Ref. 28.

It is of great interest to quantify and to compare the light-trapping potential inherent in periodic structures of different geometry. Unfortunately, the above-mentioned results are difficult to compare because they are applied to different cell configurations using various materials and methodologies. We present here a joint comparison of all the above mentioned structures, including three novel structures, applied to the same model. This allows for a reasonable comparison of the structures. Furthermore, the structures are compared both at normal and oblique angles of incidence, which is important for outdoor conditions of non-tracking solar cells. Finally, we present an analysis of the far-field diffraction pattern of the optimized structures at a wavelength of 1 μm. In contrast to standard thin-film solar cells, light trapping in a 20 μm thick Si cell involves primarily a narrow wavelength region around this wavelength. A crystalline Si slab with 20 μm thickness is used as a model in this work; however, the methodology and analysis may also hold for solar cells with other thicknesses and for other material types.

III. MODEL STRUCTURE

We have investigated numerically seven different bi-periodic structures with square lattices. The structures are cylinder, cone, dimple, inverted pyramid, roof-mosaic, rose, and zigzag structure. The unit cells of each structure are shown in Fig. 1. To simplify the representation of the zigzag and roof-mosaic structure, we have used a unit cell in the computations with twice the area of the primitive unit cell. Figure 1 shows both the computational and the primitive unit cell of these structures.

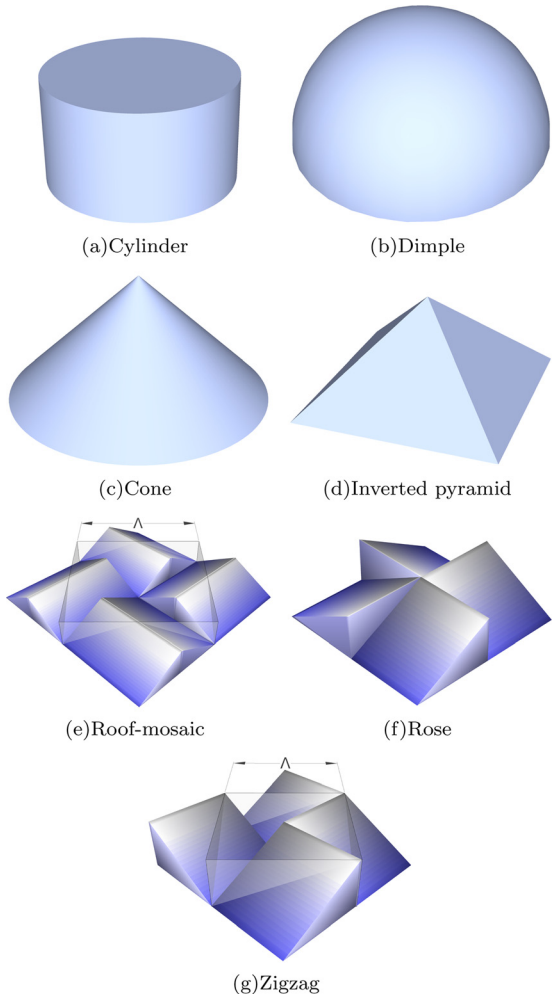

FIG. 1. (Color online) The geometry composing the unit cells of each of the investigated periodic light-trapping structures. For the roof-mosaic and the zigzag structure, Λ illustrates the lattice period of the primitive unit cell.

The full optical model of the solar cell used in the computations is depicted in Fig. 2. A 20 μm thick Si slab is covered with a planar front-side anti-reflection coating (ARC) consisting of 78 nm silicon nitride. A dielectric grating, a silicon oxide layer, and an aluminum (Al) reflector constitute

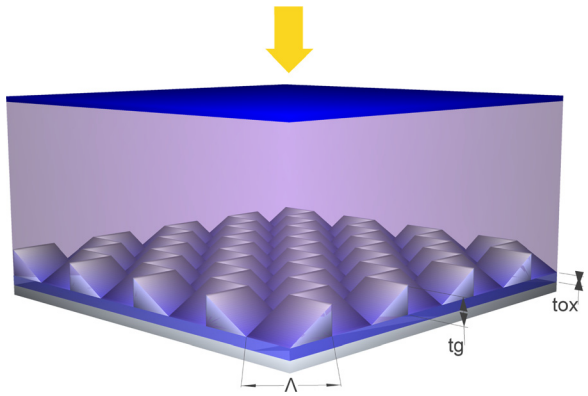

FIG. 2. (Color online) Schematic drawing of a typical optical solar cell model used in the simulations (not to scale). The Si slab has an anti-reflection coating on the front side; on the back side it has a dielectric bi-periodic grating filled with silicon oxide. The grating layer is separated from a back-side aluminum reflector by a layer of silicon oxide.

the rear side of the model. The grating is constructed from the geometries in Fig. 1, imprinted into the Si slab, and filled with silicon oxide. The purpose of the silicon oxide layer that separates the grating from the Al reflector is to reduce parasitic absorption losses in the Al. The oxide used in the separating layer and in the grating could, in principle, be replaced by another material with a low refractive index, such as air. However, silicon oxide has good passivation qualities, and there exists well known methods to make contacts through such a layer.[29] Both properties are important in a real solar cell configuration.

IV. METHODOLOGY

Modeling is performed using rigorously coupled wave analysis (RCWA).[30] With RCWA, the Maxwell equations are solved rigorously at each wavelength and the computation at each wavelength is performed independently. Experimental data for optical properties are, therefore, easily implemented and are used for Si[31] and for Al.[32] For convenience, both the ARC and the oxide layer are assumed to be non-absorbing with a refractive index of 1.95 and 1.5 representative for silicon nitride and silicon oxide, respectively.

The software package GD-Calc[33] is used as the modeling tool in this work. GD-Calc represents all types of geometries with rectangular blocks. This implies that circular structures, like the cylinder structure, are approximated by a finite number of blocks. The same holds for oblique structures, like the pyramids, which are also represented by a finite number of blocks. In the case of oblique structures, this is known as the staircase approximation.[34]

A. Grating design considerations

The most important property of the grating structure is its ability to scatter light efficiently into oblique angles, thereby extending the path length of the light inside the absorbing material. The angles of the diffracted orders can be found from the bi-periodic grating equation.[34] The polar angle of the diffracted orders θ_o can be found from Eq. (1).

$$sin^2(\theta_o) = \left(\frac{n_i}{n_o} sin(\theta_i) cos(\phi_i) + \frac{m_x \lambda}{n_o \Lambda_x}\right)^2 + \left(\frac{n_i}{n_o} sin(\theta_i) sin(\phi_i) + \frac{m_y \lambda}{n_o \Lambda_y}\right)^2. \quad (1)$$

The angles and lattice periods of Eq. (1) are defined in Fig. 3. θ_i and ϕ_i are the polar and azimuth angles of the incident beam respectively, Λ_x and Λ_y are the lattice periods in the x- and y-direction, λ is the wavelength of light in vacuum, while n_i and n_o are the refractive index of the medium of incidence and of the outgoing wave, respectively. For a reflection grating $n_o = n_i$. m_x and m_y are integers that denote the diffraction order in the x- and y-direction. The number of allowed diffraction orders is determined by the fact that the outgoing wave vector must lie on the same unit sphere, depicted in Fig. 3, as the incoming wave vector. Consequently, the expression on the right side of Eq. (1) needs to

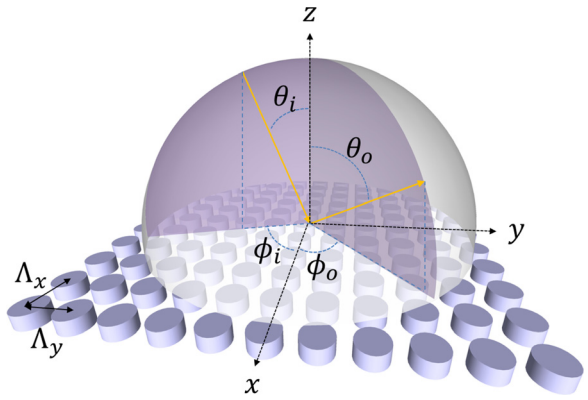

FIG. 3. (Color online) Definitions of the angles involved in diffraction from a bi-periodic grating.

be less than unity to provide a real solution (i.e., a propagating diffraction order).

For normal incidence with lattice period $\Lambda_x < \frac{\lambda}{n_o}$ and $\Lambda_y < \frac{\lambda}{n_o}$, there exists only one solution to the bi-periodic grating equation, namely the zero diffraction order $m_x = m_y = 0$. In this case, the grating will act as a specular reflector and will, therefore, not be suited for light trapping. Larger periods will allow for more diffraction orders; however, the angles of the diffracted orders will decrease with increasing period, thereby reducing the potential path-length enhancement of the lowest diffraction orders. When Λ exceeds the free-space wavelength λ, the lowest diffraction orders may also propagate in air. Therefore, these diffraction orders will not be totally internally reflected within a periodically patterned slab, regardless of the refractive index of the slab, and the light-trapping ability will be reduced.

The grating equation can only predict the angles of diffraction, while rigorous modeling must be performed to find the power distributed in each order. To optimize each structure for light trapping, we varied the lattice period Λ, grating thickness t_g, and oxide layer thickness t_{ox} (see Fig. 2). For the cylinder structure, we also varied the fill factor, i.e., the fraction of the cylinder base area to the total unit cell area, while for the rest of the geometries, the fill factor was set as large as possible without overlapping the neighboring unit cells. We chose not to confine the pyramid structure to the standard 54.7 degree angle, which is the side angle of the pyramids that are formed from alkaline etching of a [100] oriented Si wafer. Consequently, the pyramidal structure also has three independent variables. The dimple structure has, by definition, $t_g \equiv \Lambda/2$ when fill factor is maximum and, therefore, contains only two independent variables, i.e., Λ and t_{ox}.

Due to the huge number of different geometries and configurations that are investigated, a method is needed to quickly locate the grating dimensions that favor light trapping. The method that we used was to have light incident directly from an infinitely thick Si superstrate, allowing the analysis of the propagating diffraction orders. Optimal grating configurations have low specular reflection and low parasitic losses in the back-side Al reflector, and, consequently, efficient coupling into higher diffraction orders, denoted D_{HO}:

TABLE I. Maximum J_{ph} achieved with various light-trapping structures made from the structures in Fig. 1, modeled with the full structure shown in Fig. 2. The grating dimensions corresponding to the maxima are also shown.

Structure	Maximum J_{ph} [mA/cm^2]	Lattice period Λ[μm]	Grating thickness t_g [μm]	Oxide thickness t_{ox} [μm]	Fill factor
Cylinders	35.6	0.7	0.23	0.2	0.6
Roof mosaic	36.1	0.92	0.3	0.4	Max
Inverted pyramids	36.2	0.95	0.325	0.1	Max
Cones	36.3	0.98	0.38	0.1	Max
Dimples	36.4	0.975	$\Lambda/2$	0.14	Max
Rose	36.8	0.95	0.4	0.1	Max
Zigzag	37.3	0.988	0.55	0.1	Max
Reference cell	30.7	—	—	—	—

$$D_{HO} = 1 - D_{00} - A_{par}. \quad (2)$$

In this equation, D_{00} is the diffraction efficiency in the zero order, i.e., specular reflection, while A_{par} is parasitic loss in the form of absorption in the Al rear reflector. The result of Eq. (2) is mapped for the independent grating variables of each structure. As long as the diffraction modes are reasonably stable within the narrow wavelength region that is partially transmitted through the 20 μm thick Si slab, such computations may be performed with a low wavelength resolution.

We have used the resulting D_{HO} maps in the initial steps to locate the optimum grating dimensions in section V A. Previous experience has shown that the peaks in the D_{HO} maps correspond with peaks in light trapping with full-structure calculations, i.e., with the absorbing 20 μm thick Si-slab on top of the light-trapping structure and incidence from air. However, the D_{HO} maps do not include effects of secondary interactions with the grating, nor do they contain any information about the angles of the diffracted orders and the distribution of light between the orders. Consequently, the actual light-trapping efficiency may still vary greatly between the peaks, even though the size of their D_{HO} is identical. The various peaks from the D_{HO} maps are, therefore, further investigated with full-structure modeling. The absorption spectra resulting from such a full-structure modeling exhibit rapid Fabry-Perot interference fringes from interference in the 20 μm Si slab. To resolve these fringes, a high wavelength resolution is needed. This leads to significantly longer computational time for a full-structure calculation than for the computation of D_{HO}.

The absorbed photo-current density J_{ph} is used as a metric to compare the light-trapping ability of the different structures. J_{ph} is calculated by Eq. (3) and corresponds to the maximum potential short-circuit density assuming a carrier collection efficiency of 100%:

$$J_{ph} = q \int_0^{\infty} A(\lambda)\Phi(\lambda)d\lambda. \quad (3)$$

Here, q is the elementary charge, $\Phi(\lambda)$ the spectral density of the photon irradiance from the global AM 1.5 spectrum,[35] and $A(\lambda)$ is the spectral absorptance, a dimensionless wavelength-dependent factor between zero and one calculated by the full-structure modeling in GD-Calc. The integration in Eq. (3) is for wavelengths from zero to infinity, but, in practice, integration was performed from 300 nm to 1100 nm. Extension of the integral outside this range increased computational time with little effect on J_{ph}.

V. RESULTS

A. Light trapping at normal incidence

Each structure has been optimized for maximum J_{ph} using D_{HO} maps to locate favorable grating dimensions and full structure calculations to explore their corresponding light-trapping potential. The maximum J_{ph} values and the corresponding grating dimensions are summarized in Table I. A 20 μm thick reference cell with a front side ARC and a back-side planar Al reflector is also included for comparison. To better appreciate the difference in light-trapping between the structures, a plot of J_{ph} versus effective optical thickness is shown in Fig. 4. The figure illustrates the path length required through a Si slab, using the same ARC as in Fig. 2, to absorb an amount of photons corresponding to a given J_{ph}. In Fig. 4, we have also included the effective optical thickness corresponding to Lambertian light trapping, limited by the same ARC as the rest of the structures in Table I.

Not surprisingly, the light trapping from the periodic structures clearly exceeds the case of the reference cell with a planar reflector and an ARC. However, the light trapping

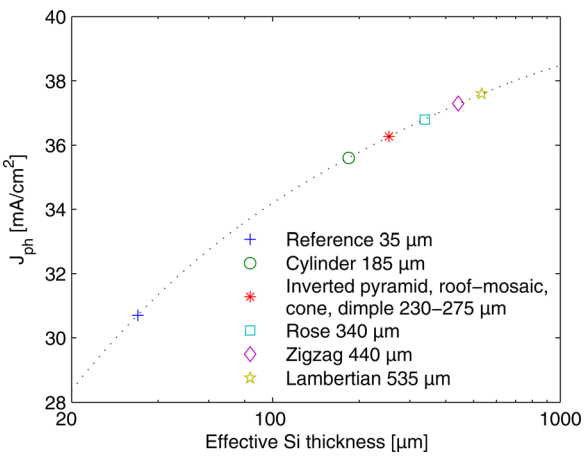

FIG. 4. (Color online) Optical thickness of Si required to provide a given photo-generated current density J_ph. The markers show the effective optical thickness corresponding to the J_ph values from Table I.

of the different periodic structures also varies significantly. We note that the best-performing structure in Table I is the zigzag structure with a J_{ph} of 37.3 mA/cm^2. This is only 0.3 mA/cm^2 below that of Lambertian light trapping. Replacing the Al reflector with an Ag reflector will further increase J_{ph} of the zigzag structure by 0.4 mA/cm^2, thereby exceeding the Lambertian light trapping at normal incidence.[24]

From Table I, we see that optimal light trapping is achieved with a lattice period of about 0.95 μm for all structures except the cylinder structure, where we found the highest J_{ph} for a period of 0.7 μm. However, as we show in Ref. 14, the cylinder structure has a broad maximum plateau extending from periods of 0.7 μm to about 1 μm, where there are only minor differences in J_{ph}.

B. Far-field analysis

To understand the differences in performance for the various light-trapping structures in Fig. 1, we explore their far-field properties. The far-field properties are shown in Fig. 5 in the form of diffraction efficiency D_{m_x,m_y} of the diffraction order m_x,m_y. The fractional power of all diffraction orders except for the zero order, i.e., $m_x = m_y = 0$, corresponds to the D_{HO} defined in Eq. (2). The allowed number of propagating diffraction orders and the corresponding diffraction angles can be found from Eq. (1).

To calculate the diffraction efficiencies in Fig. 5, we have used Si as an incidence medium. We found the diffraction efficiencies to be reasonably stable within the spectral region that is transmitted through a 20 μm thick Si slab, i.e., ~800–1100 nm. Consequently, the diffraction maps shown in Fig. 5 are representative for the entire spectral region. After verifying convergence with more diffraction orders, we included diffraction orders up to $|m_x| < 10$ and $|m_y| < 10$ in the computations. We still show only the diffraction orders up to $|m_x| < 3$ and $|m_y| < 3$, as all higher orders are evanescent, i.e., their diffraction orders hold zero power.

Figure 5 shows the diffraction efficiency for each structure in Fig. 1 when optimized for light trapping. The optimized structures each have low D_{00} and low parasitic absorption in the Al reflector, yielding D_{HO} in excess of 90% for all the structures. The distribution of power within the different diffraction orders, however, varies considerably.

The incident light in Fig. 5 is chosen to be circularly polarized, since this choice of polarization provides rotational symmetry. The diffraction efficiencies of all structures can be seen to have four-fold rotation symmetry. The exception is the diffraction pattern of the zigzag structure, which has no apparent symmetry. For the rose structure, we show the diffraction efficiencies for both left- and right-handed polarized light. Both diffraction patterns can be seen to exhibit a four-fold rotational symmetry, but the distribution of power within the diffracted orders are completely different for the two polarizations. For the rest of the structures, on the other hand, left- and right-hand polarizations yield equivalent diffraction patterns, but mirrored about the x- and y-axis (not shown). The exception is again the zigzag structure, where the diffraction pattern is mirrored only about one of the axes and not the other.

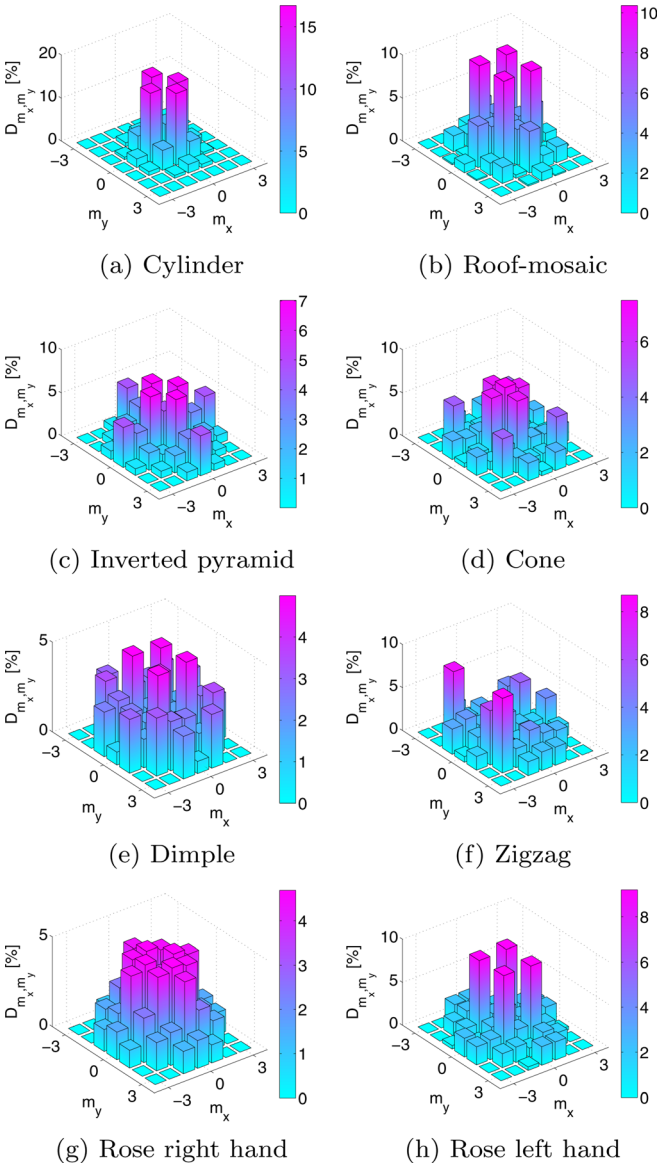

FIG. 5. (Color online) Diffraction efficiencies for circularly polarized light with $\lambda = 1$ μm at normal incidence. The diffraction efficiency of the rose structure is shown for both left- and right-handed polarization. Each structure is optimized for maximum J_{ph}, with the dimensions and corresponding J_{ph} shown in Table I. Note that the scale of the vertical axis varies between the figures.

C. Oblique incidence

The incidence angle of the solar illumination varies during the course of a day according to season and location. Moreover, diffuse radiation also makes a significant contribution to the global irradiance in several parts of the world. The properties of diffraction gratings are naturally dependent on incident angle. The behavior under oblique illumination conditions is, therefore, an important part of the performance investigation of such structures.

The light-trapping efficiency will, in general, depend on the azimuth angle ϕ in addition to the polar angle, here defined as the incidence angle from air θ_{air}. The energy that is actually captured by a solar module will, in reality, depend on the projected area of the solar module as $cos(\theta_{air})$. This

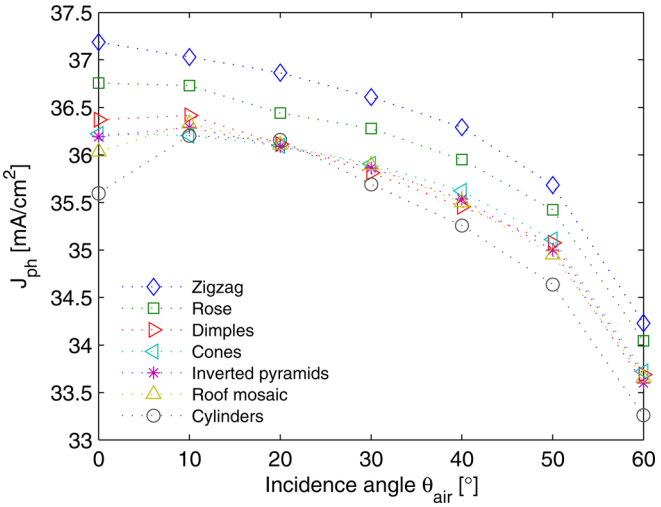

FIG. 6. (Color online) Performance of the different light-trapping structures from Fig. 1 under oblique incidence illumination. Each point represents an average of the photo-generated current density J_{ph} over two azimuth angles (four for the zigzag structure) and over s- and p-polarized light at each azimuth angle.

geometric factor is here omitted to better compare the actual light-trapping efficiency at the various angles of incidence.

All structures we investigated, except for the zigzag structure, have four-fold rotation symmetry. Dependence on θ_{air} is, therefore, studied at the two extreme azimuth angles: at $\phi = 0°$, along one of the directions of periodicity, and at $\phi = 45°$. Due to the lack of symmetry of the zigzag structure, it is characterized at four different azimuth angles: 0°, 45°, 180°, and 225°. Equivalent results were achieved for the zigzag structure at azimuth angles of 90°, 135°, 270° and 315°. In Fig. 6, the average J_{ph} of each structure is shown as a function of the angle of incidence in air above the solar cell.

The behavior of the structures in Fig. 6 may be divided into four classes by their performance. The zigzag structure is superior at all angles of incidence, while the rose structure is a clear number two. The third class consists of the dimple, cone, inverted-pyramid, and roof-mosaic structure, which are all quite similar in their performance. The fourth and last class, with the lowest performance at normal incidence, is the cylinder structure. The performance of this structure, however, increases significantly compared to the rest of the structures for non-normal angles of incidence. In general, the difference in light trapping between the structures is somewhat lower at higher angles of incidence than for normal incidence.

The reduction in J_{ph} at higher angles of incidence is primarily due to increased front-side reflection of s-polarized light. However, this does not explain the variation between the different light-trapping structures.

An important mechanism at oblique angles of incidence is the escape of diffraction orders that are no longer totally internally reflected within the Si slab. Consider the case of light with a wavelength of 1 μm incident from air on a Si slab with a back-side periodic structure having a lattice period of 0.95 μm. In this case, Eq. (1) may be used to find the allowed number of propagating diffraction orders in air by setting $n_i = n_o = 1$ and $\theta_i = \theta_{air}$. For incidence in the plane of periodicity ($\phi = 0°$), this will yield one escaping diffraction order in addition to the zero order for incidence angles $\theta_{air} > 5°$. For incidence in the $\phi = 45°$ plane, on the other hand, Eq. (1) yields up to three escaping diffraction orders in addition to the zero order. The angular response for incidence in the $\phi = 0°$ plane may, therefore, be expected to exceed the response at $\phi = 45°$. In fact, this trend is evident for all structures except for the cylinder structure. With a period of only 0.7 μm, Eq. (1) will show that incidence in the $\phi = 45°$ plane does not allow any escaping orders except the zero order as long as the wavelength is above 1 μm. Consequently, the cylinder structure has a better angular response for $\phi = 45°$ than for $\phi = 0°$ (not shown). Additionally, due to the smaller lattice period of the cylinder structure, an incidence angle $\theta_{air} > 20°$ is needed before any higher diffraction orders may escape.

The analysis above is a qualitative approximation, as we consider only a single wavelength of the extended spectrum that reach the back side and we neglect the fact that the diffraction efficiencies will also change with incidence angle. Nevertheless, the main difference that can be observed between the grating structures may, in large part, be explained by this simple analysis.

VI. DISCUSSION

A. Interpretation of results

In general, a low zero-order diffraction efficiency is a prerequisite for good light trapping, and, indeed, the zero-order diffraction efficiencies in Fig. 5 fulfill this requirement. Furthermore, high diffraction angles will increase path length more than low diffraction angles. For a grating with a given lattice period, this implies that coupling to higher diffraction orders is better for light trapping than coupling to lower orders (see Eq. (1)). Nevertheless, the photo-generated current density J_{ph} of the dimple structure is below that of the rose structure, even though the dimple structure seems to have larger part of its diffracted power in the highest diffraction orders. The reason for the success of the rose and the zigzag structure must, therefore, be caused by another effect.

Our first assumption for the success of the rose and the zigzag structure was that the number of sharp edges and corners in these structures increased scattering and, therefore, light trapping. However, the roof-mosaic structure also has several sharp corners, yet it has significantly lower J_{ph}. A further investigation of Fig. 5 reveals that the symmetry in the diffraction patterns of the two structures having the highest J_{ph} differs from the rest of the structures. The diffraction pattern of the zigzag structure has no symmetries, while the rest of the structures show a four-fold rotational symmetry. By reversing the direction of the circularly polarized light, we found that the diffraction patterns are reproduced, but mirrored about the x- and y-axis. The exceptions are for the zigzag and the rose structures. The diffraction pattern of the zigzag structure is only mirrored about one axis. The diffraction pattern from the rose structure is completely changed with polarization, although it still exhibits a four-fold rotational symmetry.

We believe that the reduced symmetry in the diffraction patterns of the rose and zigzag structure in Fig. 5 reduces the

chance of out-coupling on subsequent interactions with the diffraction grating. This argument is similar in nature to the one of Ref. 9. The results we see here also match well with what has been suggested recently by Refs. 16 and 18. They suggest that to break the symmetry of the unit cell will allow the coupling to more modes, thereby increasing light trapping.

B. Implementation in solar cells

To obtain success with a periodic light-trapping structure, it is important to avoid the excessive absorption that may arise in the metal reflector that is usually placed on the back side of a solar cell. We reduce the parasitic absorption with an oxide layer that separates the rear reflector from the grating. In this work, we use a planar metal reflector. Absorption is expected to be higher if the grating structure is transferred to the Al.[36,37] Other approaches with Bragg reflectors have also been proposed to avoid parasitic absorption.[12,13] We find that a separation of the grating and rear reflector is necessary, not only for Al, but also for a less absorbing Ag reflector.

A low back-surface recombination velocity is crucial to obtain high efficiency with thin solar cells, where diffusion length may be several times the thickness of the cell. Improper surface passivation has been shown to be a barrier for the successful implementation of back-side diffractive structures in solar cells.[36] The oxide layer used in this model may serve as a back-side passivation layer. In principle, a thin planar optically inactive oxide layer may be inserted between the grating layer and the bulk Si to further reduce surface recombination.

From Fig. 4, we see that the best structures are not far from a Lambertian surface when it comes to light confinement. However, for these structures, the largest loss mechanism is no longer incomplete absorption, but instead the front-side reflectance from the single layer ARC. The front-side reflectance is also mainly responsible for the reduced performance of all the structures at higher angles of incidence (see Fig. 6).

Front-side pyramidal textures are commonly used in today's solar cells. For short wavelengths that do not penetrate to the back side, a front-side texture will certainly increase light absorption by reducing front-side reflectance. The effect of a grating in combination with a textured front surface is, of course, much smaller than for a planar front surface. The exact effect on light confinement for long wavelengths are difficult to predict, since a front-side texture will change the incident angles and affect the light trapping from a back-side grating. Such macroscopic structures are difficult to model rigorously and are outside the scope of this work. Such computations could, in principle, be performed using a combination of ray-tracing and RCWA.[37]

In a solar module, the solar cells will be encapsulated with glass on the front side. Since the light reflected from a Si-glass interface is lower than from a Si-air interface, the advantage of a front-side texture over that of a planar cell will be somewhat reduced with encapsulation compared to the case without encapsulation. Nevertheless, to further increase absorption, a lower front-side reflectance is required. Multiple or graded ARCs are possible solutions that will conserve the light-trapping ability of the back-side periodic structures and, at the same time, reduce front-side reflectance.

Fabrication of sub-micron periodic structures on large areas is obviously not trivial. Some techniques that might have potential for large scale production include nano-imprint lithography or hot embossing[38,39] and interference (holographic) lithography.[38,40] Self-assembled structures are yet another possibility. One example of this is a periodic dimple structure with a triangular lattice that has been realized by anodic etching of Al.[22] The different geometries in this work may have various possibilities for fabrication. Nobody has fabricated structures like the rose and zigzag structure today, and large area fabrication of such structures will not be a simple task. Hopefully, low-symmetry light trapping structures that lend themselves to fabrication may be designed.

The structures presented in this work are all subject to the limitation that they require patterning of Si (or another high index material). The grating does not necessarily need to be filled with an oxide. A grating consisting of Si and air could, in principle, provide a more broad-banded response than a Si-oxide grating because of the larger refractive index contrast.

VII. CONCLUSION

We have optimized and compared the light-trapping potential of seven different periodic structures with essential differences in the geometry of their unit cells. The geometries comprise the cylinder, inverted pyramid, cone, dimple, roof-mosaic, rose, and zigzag structure. We found that the optimized structures had similar lattice periods despite their difference in geometry. The light-trapping potential of the structures range from a photo-generated current density J_{ph} of 35.6 mA/cm^2 for the cylinder structure, corresponding to an effective optical thickness increase of a factor of 9, to a J_{ph} of 37.3 mA/cm^2 for the zigzag structure, corresponding to an increase in optical thickness of a factor of 22.

Analysis of the diffraction patterns revealed that the two structures with the highest J_{ph} have less symmetry than the rest of the structures. The best light trapping is achieved for the least symmetric of the structures. This agrees well with literature, which suggests that non-symmetric structures are superior to symmetric ones. The light trapping achieved with the zigzag structure is close to that of the Lambertian limit, in spite of the fact that the zigzag structure makes use of the strongly absorbing Al as reflector material.

The investigation at oblique angles of incidence shows that the back-side gratings perform well at angles of incidence up to 60 degrees, also when considering an average over several azimuth angles and both polarizations. The reduced performance at higher angles of incidence is dominated by the increase in front-side reflectance of s-polarized light from the planar ARC.

The comparison we present in this work is applied to a 20 μm thick Si slab, but the light-trapping structures, as

such, are not constricted to a certain material or thickness. We have used Si as a case of study, since the poor absorption of Si makes light trapping specifically important. A different choice of thickness or material is expected to change the optimal grating dimensions. Particularly, the optimal lattice period is expected to be reduced for thinner solar cells, where a broader spectrum will reach the back side.

ACKNOWLEDGMENTS

The authors would like to acknowledge the Norwegian research council through the program Nordic Center of Excellence in Photovoltaics (NoCEPV).

[1]A. W. Blakers, K. J. Weber, M. F. Stuckings, S. Armand, G. Matlakowski, A. J. Carr, M. J. Stocks, A. Cuevas, and T. Brammer, Prog. Photovoltaics **3**, 193 (1995).
[2]K. Feldrapp, R. Horbelt, R. Auer, and R. Brendel, Prog. Photovoltaics **11**, 105 (2003).
[3]F. Henley, A. Lamm, S. Kang, Z. Liu, and L. Tian, in *Proceedings of the 23rd European Photovoltaic Solar Energy Conference*, Valencia, Spain, 1–5 September 2008.
[4]A. Luque and S. Hegedus, *Handbook of Photovoltaic Science and Engineering* (Wiley, New York, 2003).
[5]D. H. Macdonald, A. Cuevas, M. J. Kerr, C. Samundsett, D. Ruby, S. Winderbaum, and A. Leo, Sol. Energy **76**, 277 (2004).
[6]D. Kray and K. R. McIntosh, Phys. Status Solidi A **206**, 1647 (2009).
[7]J. Müller, B. Rech, J. Springer, and M. Vanecek, Sol. Energy **77**, 917 (2004).
[8]M. Gale, B. Curtis, H. Kiess, and R. Morf, Proc. SPIE **1272**, 60 (1990).
[9]C. Heine and R. H. Morf, Appl. Opt. **34**, 2476 (1995).
[10]P. Sheng, A. N. Bloch, and R. S. Stepleman, Appl. Phys. Lett. **43**, 579 (1983).
[11]C. Haase and H. Stiebig, Prog. Photovoltaics **14**, 629 (2006).
[12]P. Bermel, C. Luo, and J. D. Joannopoulos, Opt. Express **15**, 16986 (2007).
[13]J. G. Mutitu, S. Shi, C. Chen, T. Creazzo, A. Barnett, C. Honsberg, and D. W. Prather, Opt. Express **16**, 15238 (2008).
[14]J. Gjessing, E. S. Marstein, and A. S. Sudbø, Opt. Express **18**, 5481 (2010).
[15]E. Yablonovitch, J. Opt. Soc. Am. **72**, 899 (1982).
[16]Z. Yu, A. Raman, and S. Fan, Opt. Express **18**, 366 (2010).
[17]A. Chutinan, N. P. Kherani, and S. Zukotynski, Opt. Express **17**, 8871 (2009).
[18]S. E. Han and G. Chen, Nano Lett. **10**, 4692 (2010).
[19]J. Gjessing, A. S. Sudbø, and E. S. Marstein, paper presented at the EOS Annual Meeting, Paris, France, 26–28 October 2010.
[20]L. Zeng, P. Bermel, Y. Yi, A. Alamariu, K. A. Broderick, J. Liu, C. Hong, X. Duan, J. Joannopoulos, and L. C. Kimerling, Appl. Phys. Lett. **93**, 221105 (2008).
[21]V. E. Ferry, M. A. Verschuuren, H. B. T. Li, E. Verhagen, R. J. Walters, R. E. I. Schropp, H. A. Atwater, and A. Polman, Opt. Express **18**, 237 (2010).
[22]H. Sai and M. Kondo, J. Appl. Phys. **105**, 094511 (2009).
[23]J. Gjessing, A. S. Sudbø, and E. S. Marstein, paper presented at Optics for SOLAR, Tucson, AZ, USA, 7–9 June 2010.
[24]J. Gjessing, A. S. Sudbø, and E. S. Marstein, J. Eur. Opt. Soc. Rapid Publ. **6**, 11020 (2011).
[25]C. Haase and H. Stiebig, Appl. Phys. Lett. **91**, 061116 (2007).
[26]D. Zhou and R. Biswas, J. Appl. Phys. **103**, 093102 (2008).
[27]S. B. Mallick, M. Agrawal, and P. Peumans, Opt. Express **18**, 5691 (2010).
[28]R. Biswas, D. Zhou, and L. Garcia, Mater. Res. Soc. Symp. Proc. **1153**, 1153-A03-02 (2009).
[29]E. Schneiderlöchner, R. Preu, R. Lüdemann, and S. W. Glunz, Prog. Photovoltaics **10**, 29 (2002).
[30]L. Li, J. Opt. Soc. Am. A **13**, 1024 (1996).
[31]C. M. Herzinger, B. Johs, W. A. McGahan, J. A. Woollam, and W. Paulson, J. Appl. Phys. **83**, 3323 (1998).
[32]Handbook of Optical Constant of Solids, edited by E. D. Palik (Academic, New York, 1985).
[33]See http://software.kjinnovation.com/GD-Calc.html for more information about the grating diffraction calculator.
[34]K. C. Johnson, *Grating Diffraction Calculator (GD-Calc) - Coupled-Wave Theory for Biperiodic Diffraction Gratings* (2006).
[35]See http://rredc.nrel.gov/solar/spectra/am1.5/for more information about the AM 1.5 spectrum.
[36]P. Berger, H. Hauser, D. Suwito, S. Janz, M. Peters, B. Bläsi, and M. Hermle, Proc. SPIE **7725**, 772504 (2010).
[37]M. Peters, M. Rüdiger, D. Pelzer, H. Hauser, M. Hermle, and B. Bläsi, in *Proceedings of the 25th European Photovoltaic Solar Energy Conference*, Valencia, Spain, 6–10 September 2010.
[38]A. Gombert, K. Rose, A. Heinzel, W. Horbelt, C. Zanke, B. Bläsi, and V. Wittwer, Sol. Energy Mater. Sol. Cells **54**, 333 (1998).
[39]M. Heijna, J. Loffler, B. Van Aken, W. Soppe, H. Borg, and P. Peeters, Mater. Res. Soc. Symp. Proc. 1101 (2008).
[40]S. H. Zaidi, J. M. Gee, and D. Ruby, in *28th IEEE Photovoltaic Specialists Conference*, Anchorage, AK, 15–20 September 2000, pp. 395–398.